# COMPARISON OF STATIONARY AND TRANSIENT RANS MODELLING TO PREDICT THE SPATIAL VELOCITY FIELD OF A CEILING INTEGRATED FAN

O. Glahn[1,2], T. Voß[2], K. Voss[2] and S. Schwickert[1]
[1]Institute Future Energy, OWL University of Applied Sciences and Arts, Lemgo, Germany
[2] Dep. Building Physics & Technical Services, University Wuppertal, Wuppertal, Germany

## ABSTRACT

Ceiling fans allow an increase of the local air velocity on the human body. The associated heat transfer increases user's temperature tolerance in warm environments.

In the presented study, the differences in the application statistical turbulence models (RANS) for modelling the air flow induced by a ceiling integrated fan is outlined with particular focus on comparing steady and transient simulations. Results of a CFD simulation (Fluent) are shown and compared with measured data of the horizontal velocity distribution.

The study shows that especially the transient simulation using the Realizable *k*-ε model follows the flow pattern described in literature. But at 1.1 m above the floor, the mean absolute error in the center of the jet is at least five times larger than the measurement uncertainty and 41 % higher than the measured values. The stationary model using the Multiple Reference Frame (MRF) approach instead, shows the smallest mean absolute error, exceeding the measured values in the center of the jet by 16%. But in the immediate vicinity of the fan an unrealistic velocity distribution can be observed, if the moving zone needs to be small due to obstacles. For a freely suspended ceiling fan, the moving zone can be adjusted accordingly and the flow pattern can be improved. But modelling a ceiling integrated fan with a fan housing and obstacles in the near region, transient simulations using rigid body motion are required for accurate results.

## INTRODUCTION

The ceiling fan spatial velocity distribution, as it is subject of this study, is part of a research field several international research groups are currently working on (Chen et al., 2018; Gao et al., 2017; Liu, Lipczynska et al., 2018; Voss & Voß, 2016; Wang, Luo et al., 2019).

The velocity field induced by a ceiling fan increases human body heat dissipation and results in a higher temperature tolerance in warm environments. Beside the velocity, field studies also analyze human perception of air velocities, using questionnaires (Brager et al., 2004; Melikov, 2004; Pasut et al., 2014; Rissetto et al., 2020; Zhai et al., 2017) and investigate the usage of ceiling fans by the occupants (Schweiker & Wagner, 2016). Other studies analyze potentials to increase night cooling (Rizk et al., 2015; Voss et al., 2013) or the control of stand fans to achieve a homogeneous velocity distribution (Liu, Le Yin et al., 2018). Another study investigated the ceiling fan blade optimization for improved aerodynamic performance (Adeeb et al., 2016).

One of the central research objectives is to derive design criteria for the integration of ceiling fans in room climate concepts. The ASHRAE is currently also developing a standard for measuring the spatial velocity distribution of ceiling fans (ASHRAE, 2018).

This study focuses on the air flow distribution of fans that are integrated in a suspended ceiling-panel and particularly emphasizes on boundary conditions for CFD simulations. Obstacles close to the rotor, like the fan housing as well as the panel, imply limitations in modelling. Methods used in literature to do CFD simulations on ceiling fans can only be applied to a limited extend. Therefore, the behavior of transient RANS modelling with rigid body motion (RBM) gets investigated for application in ceiling fan CFD modelling.

### Thermal Comfort

Increased air velocities enhance the convective heat dissipation and evaporation of the human body. (Arens et al., 2009; Tanabe & Kimura, 1994). From an air speed of approx. 0.1 m/s, free convection is superposed by forced convection and the heat flow increases (Fanger, 1970; Melikov, 2004). At seated activity (MET 1.3) and summer office clothing (CLO 0.7: e.g. long trousers, shoes and shirt), air velocities can also be perceived from as low as 0.05 m/s (Brager et al., 2004). Furthermore the evaporation on the human body increases exponentially degressively with increasing air velocity (Candas et al., 1979).

Studies show that an environment with 27.5-30 °C and air velocities of 0.8-1.0 m/s can be perceived as comfortable (Huang et al., 2013; Rohles et al., 1982; Xia et al., 2000; Zhai et al., 2017). It can be deduced from this, that controlling the air speed in warm environments can increase the thermal comfort band and thus offer potential for energy savings. In cool to mild summer climate regions (Berlin, Helsinki) air velocities of up to 0.8 m/s can be expected to save 34 % - 48 % of net cooling energy in total, depending on

 DOI: 10.3217/978-3-85125-786-1-11 

the temperature setpoint (Schiavon & Melikov, 2008). Besides that, ceiling fans enable the compensation of active cooling in German summer climate regions, as long as no extreme summer conditions prevail. This allocates additional savings in investment and operation costs. (Glahn, 2016)

To avoid draft, it is recommended to keep velocities below 0,8 m/s to 1,0 m/s. Therefore the operative room temperature, which is still considered comfortable, can thus be increased by a maximum of 3 K. (Cândido et al., 2011; Pasut et al., 2014; Rohles et al., 1982). These requirements are also considered in current international standards (ASHRAE Standard 55-2017; DIN EN 16798-1:2015-Draft; DIN EN ISO 7730:2006-05; DIN EN 15251:2012-12). However, studies show that under very warm conditions (>28 °C), higher air speeds of up to 1.4 m/s can also be perceived as comfortable (Zhai et al., 2017).

The thermal sensation between different body regions varies significantly (Y. Zhang & Zhao, 2007). Ceiling fans offer a more homogeneous velocity field compared to table and stand fans. Therefore they are perceived as more comfortable than other systems. (Schiavon & Melikov, 2009)

In consideration of the individual thermal perception, that could differ significantly between occupants (de Dear & Brager, 1998; Kim et al., 2019; Nicol & Humphreys, 2002), especially systems that enable control over individual comfort conditions are of particular interest. These systems have high potential in improving thermal comfort perception as well as energy consumption. Furthermore it can be expected, that the opportunity of individual occupant control results in further, psychologically driven, comfort effects (Brager et al., 2004; Luo et al., 2016). Therefore, systems that influence only a single workplace and not the air speed at the adjacent workplaces appear to be most interesting. In that consideration, this study focuses on ceiling fans with a diameter of 30 cm.

**Airflow pattern induced by ceiling fans**

The spatial airflow distribution, induced by the ceiling fan can be assigned to have the characteristics of a free shear flow. Here the jet width increases proportional to the fan distance. The jet reduces the speed with increasing distance and at the same time carries along new still air from the surrounding (Oertel & Prandtl, 2017). Based on this instance, the air flow pattern can be characterized in different zones, whereas the explicit velocity field within the jet is influenced by the blade rake and rotational speed (Aynsley, 2007).

In Wang, Luo et al. (2019) and Wang, Zhang et al. (2019) the characteristic velocity distribution based on a "color sequence particle streak velocimetry" (CSPSV) is divided into six zones as follows. There is the jet core, with the maximum velocities increasing radially from the center to the outer diameter of the fan. Adjacent to the jet is the entrainment zone where the ambient air is entrained by the jet. Near the floor the air flow spreads in the spreading zone. From there the air moves towards the wall and flows within the wall zone upwards. In the room between the jet and the wall is the recirculation zone. Within that zone the air flows from the wall back towards the floor and circulates. The sixth zone is located above the ceiling fan and is called suction zone. Comparable characterizations can also be found in Liu, Lipczynska et al. (2018) and Gao et al. (2017).

**Review of methods for modelling a ceiling fan induced velocity field**

The principal challenge in modeling turbulent flows is to achieve representative results with adequate computing effort. Consequently, statistical turbulence models (RANS) have been used in all reviewed works that executed numerical investigations on ceiling fan velocity fields. The turbulence models available in commercial CFD programs are based on certain assumptions and are therefore not equally suitable for all types of flows found in a room. The behavior of different turbulence models in enclosed environments is summarized in Z. Zhang et al. (2007). There, the v2f-dav and the RNG $k$-ε show the best accuracy for flows with forced and mixed convection.

When modelling a ceiling fan in a room, several forms of turbulent flow can be found. Consequently, a single turbulence model can only be used to a limited extent.

The flow at the blade corresponds to the flow around a body and requires a precise, spatially high-resolution calculation of the boundary layers and wall turbulence. The outflow into the empty space is characterized by a free shear flow, which has large Reynolds numbers in the center of the jet, that decrease with increasing distance from the fan as well as in width. In addition, the momentum emanating from the fan contains swirl components that influence this free shear flow. Another factor that influences the flow distribution is the floor or any furniture. As an obstacle, these deflect the jet, so that a calculation of the boundary layer near the obstacle is necessary.

Although the boundary conditions of a rotating fan are transient, most CFD analyses are based on stationary calculations (Adeeb et al., 2016; Casseer & Ranasinghe, 2019; Chen et al., 2018; H.-H. Lin, 2019; S.-C. Lin & Hsieh, 2014; Momoi et al., 2004; Zhu et al., 2014). Here, the rotation was usually modelled via a Multiple Reference Frame (MRF). In Momoi et al., 2004 instead, a measured flow field both below and above the fan was imposed as a boundary condition.

In Babich et al. (2017) a transient simulation was performed, but without considering the fan geometry. The momentum was implemented in the model as a source in the form of a rotating ring.

The turbulence models used in these studies differ. In Bassiouny and Korah (2011), Chen et al. (2018), H.-H. Lin (2019), S.-C. Lin and Hsieh (2014) and Momoi et al. (2004) the Standard $k$-ε was used; in Zhu et al. (2014) and Franzke and Sebben (2018) instead, the Realizable $k$-ε model was applied. According to

 DOI: 10.3217/978-3-85125-786-1-11 

ANSYS (2017) the Realizable $k$-ε model has substantial benefits in calculating rotating flow structures compared to the Standard $k$-ε model.

In Adeeb et al. (2016) the Spalart-Allmaras turbulence model showed the best agreement with velocity measurements at 1.5 m distance from the fan. This was compared with the Standard $k$-$\varepsilon$ and the $k$-ω model. Casseer and Ranasinghe (2019) came to the same result, where the Spalart-Allmaras turbulence model also shows the best agreement with the axial velocity measured at the end of a round duct compared to the Standard $k$-ε, RNG $k$-ε, as well as $k$-ω model.

In the transient calculation considering the fan as a momentum source, the Shear Stress Transport $k$-ω (SST $k$-ω) model showed advantages over the Standard $k$-ε, RNG $k$-ε, as well as $k$-ω model (Babich et al., 2017).

**Reflection and Objective**

Summarizing these studies, the Realizable $k$-ε, the SST $k$-ω model as well as the Spalart-Allmaras turbulence model are from particular interest to model ceiling fans and their spatial velocity field in a room.

Even the v2f-dav model is recommended for flows with forced and mixed convection (Z. Zhang et al., 2007), there is no experience found in the application of the v2f-dav model with rotating fans. Therefore, it is not further investigated in this study. Furthermore, the Spalart-Allmaras is also not considered further in this study because it is not calibrated for free shear flows according to ANSYS (2017).

The Realizable $k$-ε model is a development of the Standard $k$-ε model, which is a two-equation model solved by the transport equations of turbulent kinetic energy $k$ and turbulent dissipation ε. The Realizable $k$-ε model was developed because experiments had repeatedly shown that the Standard Model does not provide realistic results for large deformations. For the Realizable $k$-ε model the equation for the dissipation rate was modified and an alternative formulation of the turbulent viscosity was introduced. Here, the constant $C_\mu$ from the Standard Model is solved by a functional relation to the deformation rate and mean rotation (Schwarze, 2013; Shih et al., 1995).

A further development of the Standard $k$-ε model is also the RNG $k$-ε model, which contains several refinements that lead to improved results in swirling flows. Principally it is suitable for a wide class of flows and contains also an additional term in the dissipation equation that improves the accuracy for rapidly strained flows. (ANSYS, 2017; Schwarze, 2013; Yakhot et al., 1992) It is also recommended for enclosed room simulation with forced or mixed convection (Z. Zhang et al., 2007). In Babich et al. (2017) and Casseer and Ranasinghe (2019) however, the RNG $k$-ε model did not show sufficient agreement with measurement results in modelling the spatial ceiling fan flow. Therefore, it will not be considered in the analyses below.

In Babich et al. (2017) SST $k$-ω model showed the best agreement with the spatial measurement in a transient ceiling fan simulation. In the following analysis the Transition SST model is used instead. This is a coupling of the SST $k$-ω transport equations with two further transport equations, one for the formulation of the intermittency and another one for the transition criteria, based on the momentum-thickness Reynolds number. The Transition SST model is optimized for mapping laminar boundary layer or boundary layer separation in a transition point. However, it is limited to wall-bounded flows and therefore not applicable for free shear flow regions, since these will be assumed to be completely turbulent according to the Standard $k$-ε model. (ANSYS, 2017)

In the available literature on modelling ceiling fans and distant spatial velocity distribution in a room, there are no transient simulations described, that consider the fan geometry and apply rigid body motion (sliding mesh). In Franzke and Sebben (2018) and Franzke et al. (2019) this method was investigated for a vertically clamped axial fan. They focused particularly on the velocity field in 4 mm distance to the fan including obstacles and a heat source close to the intake and outlet. But the distant spatial velocity field in the room has not been examined. They concluded in their study, that the MRF approach shows non-physical behavior in the downstream region and that a larger rotating zone could improve that behavior. But this is not possible, if stationary parts like a ceiling panel or a housing surrounds the fan. Furthermore, most of the existing studies used freely suspended ceiling fans with a diameter of 1.2-1.4 m. In this study instead, a fan with a diameter of 30 cm, integrated in a ceiling panel is examined in order to analyze the potential of individual control due to the narrow region of influence.

## SIMULATION AND EXPERIMENT

The main focus of the analysis is the methodological comparison of different RANS models to predict the velocity distribution of a ceiling integrated fan.

**Measurements**

Measurements of the radial velocity field in 1.1 m above the floor (head of a seated person according to EN ISO 7726:2001) are used to validate the results in the relevant occupied zone. The fan speed was set to 265 rpm to have a maximum mean velocity of approx. 0.6 m/s in the occupied zone. The measurements were performed in an empty room (54 m²). The fan was mounted centered in the room with a radial distance of approx. 3.57 m to surrounding walls. During the measurements there were no flow obstacles or thermal loads in the room and no ventilation was performed. The ceiling panel with the fan was suspended at a distance of 2.5 m from the floor. To limit the suction zone compared to a real office situation with a room height of approx. 2.8 m, an additional panel (size: 1.5 m x 1.2 m) was placed at a distance of 20 cm above the fan, 28 cm above the panel respectively (see Figure 1). Comparing with simulation results (see figure 3) it

 DOI: 10.3217/978-3-85125-786-1-11 

is expected that this additional panel covers the entire suction zone with air velocities above 0.1 m/s. Nevertheless, it allows only an indicative transferability to an office room with a room height of 2.8 m.

*Figure 1: Measurement Setup (University Wuppertal)*

The air velocity was measured with 8 omnidirectional hot-wire anemometers of the type FV A605 TA1 (Ahlborn) (measuring range 0.01 to 1 m/s; accuracy ±1 % of the final value and ±1.5 % of the measured value). These were mounted with a distance of 20 cm. Eight radial measurement series with an angular distance of 45° were taken. Two measurements were carried out for each position using two different sensors (measurement duration: 5 minutes with a sample frequency of 300 ms). The mean of the mean velocity from these radial measurement series is plotted in figure 2 assuming a symmetrical distribution and accounting corresponding deviations in the experimental uncertainty (displayed as error bars).

The experimental uncertainty $u_D$ is based on the systematic standard uncertainty calculated according to (ASME V&V, 2009).

$$u_D = b_v = \sqrt{b_{v\,cal}^2 + b_{v\,sens}^2 + b_{v\,env}^2} \quad (1)$$

With the systematic standard uncertainty for velocity $b_v$, the calibration uncertainty $b_{v\,cal}$, the conceptual uncertainty from the sensor setting $b_{v\,sens}$ and the conceptual uncertainty from the environment $b_{v\,env}$.

Due to the turbulent flow, the standard deviation of the measurement series could not be used to describe the measurement uncertainty. Therefore, the conceptual uncertainty is estimated by taking multiple measurements of a position or radial distance and calculating the standard deviation of the different mean velocities.

For $b_{v\,sens}$ test measurement series were taken with all applied sensors during fan operation at selected positions with a duration of 9 min and a sample rate of 300 ms. The uncertainty is derived from a corresponding regression curve, based on a function of the absolute mean air velocity. For $b_{v\,env}$ the standard deviation of mean velocities for each radial distance from the radial measurement series were used to account deformations in the velocity distribution due to environmental impacts. For example, these could be air leakages at the façade, pressure differences to neighboring rooms or uncertainties in mounting the panel and fan.

**Geometry and Mesh**

The simulation model is based on the measurement environment. For simplification and transferability to office situations, a homogeneous ceiling with 28 cm distance to the panel got implemented. Compared to the measurements, uncertainties could arise, because the experimental setup only considered this lower ceiling to a limited extend.

The fan model is based on a 3D scan with an Artec Eva scanner (nominal 3D point accuracy: 0.1 mm). The fan geometry in the CFD model did not include the protection cover underneath the rotor in order to reduce meshing effort and calculation time.

For the study a model is used with a mesh of 2.84 million tetrahedral and hexahedral cells. The minimum orthogonal quality is 0.136. The fan is meshed with an element size of 0.5-4 mm. The cell sizes of the other regions vary according to the expected speed gradients (underneath the fan: 5 mm, the panel cutout: 1 cm, the space underneath the panel: max. 4 cm, enclosing space max. 7.5 cm, above the fan max. 5 cm; max. growth rate: 1.2).

In addition, a mesh sensitivity analysis was performed using a mesh that was 1.4 times finer in each of the distinctive regions. A mesh-dependent error of up to 10 % was found in the center of the fan. However, the focus of this study is on methodological comparison, so that the initial mesh was considered sufficient.

**Boundary Conditions CFD Simulation**

The simulations were performed with the Ansys Fluent software (version 19.2). The different models, that were considered in the course of the investigation, are summarized in Table 1.

Steady-state and transient modelling will be compared using RANS models in order to highlight the differences when the transport equations for each time step of a rotor motion are solved. The MRF method is used in the steady-state calculation. In the transient solution the fan is modeled in form of the Rigid Body Motion (RBM), also called sliding mesh.

 DOI: 10.3217/978-3-85125-786-1-11 

*Table 1: Model Conditions*

| | TIME | RANS | PRESSURE |
|---|---|---|---|
| V1 | steady | Realizable $k$-ε | SIMPLE |
| V2 | | | Coupled |
| V3 | transient | | SIMPLE |
| V4 | | | Coupled |
| V5 | | Transition SST | PISO |

In addition, differences between the SIMPLE pressure correction equation and the coupled solution in the relevant flow areas are outlined. In general, it can be assumed that the simultaneous solution of the flow variables (velocity, pressure, enthalpy and temperature) takes better account of the interactions of the corresponding variables. So, rotating objects should be better represented. With the exception of Adeeb et al. (2016), sequential solutions were always used in the available studies (with documented pressure solution). A corresponding comparison could not be taken from the available literature.

In order to build on the experience from the summarized literature in the introduction about modelling ceiling fans, the Realizable $k$-ε model is selected to compare steady and transient methods. The Transition SST was selected additionally for this study to analyze and compare it with the Realizable $k$-ε model in modelling the blade velocity profile.

In the Realizable $k$-ε model the mean rate of rotation tensor contains an additional rotation term $(-2\varepsilon_{ijk}\omega_k)$, which can lead to incorrect results in simulations with rotating objects, so that this additional term was deactivated for the simulations considered here (ANSYS, 2017). The near wall region has been modelled using the "Enhanced Wall Treatment". Here, the whole domain is subdivided into a “viscosity-affected region and a fully-turbulent region” by a wall-distance-based turbulent Reynolds number. These regions are solved separately and blended by means of a two-layer formulation (ANSYS, 2017).

## ANALYSES AND DISCUSSION OF RESULTS

### Results

The simulations show that the blade geometry of the rotor leads to a center-directed velocity vector at the given rotational frequency, so that the low velocity field in the center of the fan is already faded after about 15 cm. Instead, the freely suspended ceiling fans investigated in other studies (Babich et al., 2017; Chen et al., 2018; Gao et al., 2017; Liu, Lipczynska et al., 2018; Raftery et al., 2019; Wang, Zhang et al., 2019) showed a centered eye of low velocities that remained until the floor.

It should be noted that the selected turbulence models are expected to have inaccuracies in the transitions between high and low Reynolds numbers. In the calculations performed with the Transition SST model, the low-speed region in the center of the jet is longer and extends up to 1 m, but predicts at 1.1 m above the floor (1.4 m underneath the fan) the highest core velocity compared to the other models (figure 2).

Figure 2 shows the axial velocities of both the simulation models and the measurement at a height of 1.1 m (above to the floor). At that section the stationary models show a better agreement with the measurements compared to the transient model. The steady state MRF calculation with the coupled solutions (V2) has the lowest mean absolute error (MAE) (see table 2).

$$MAE = \frac{\sum_{i=1}^{n}|v_D - v_S|}{n} \quad (2)$$

($v_D$: mean velocity experiment [m/s]; $v_S$: mean velocity simulation [m/s]; $n$: count of positions)

But V2 still exceeds the experimental uncertainty ($u_D$) in the center of the jet (within a diameter of 20 cm) by 0.07 m/s, thus exceeds the measured velocity including the uncertainty by 16 %. The transient solution with the SIMPLE pressure correction (V3) instead exceeds the measured velocity by 41 % in the center of the jet. In the outer zone the MAE of all models is lower or equal $u_D$ (see table 2).

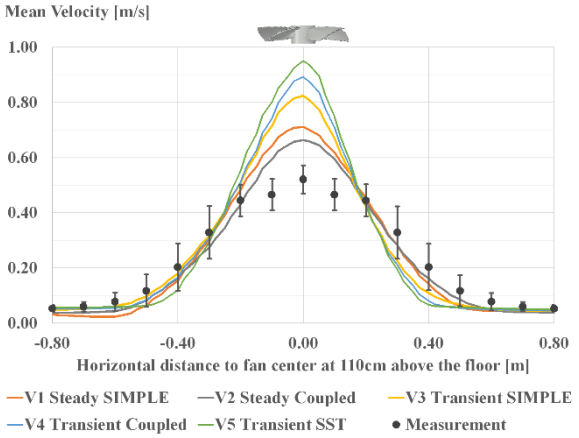


*Figure 2: Velocity distribution at 1.1 m above the floor (1.4 m underneath the fan)*

However, in the axial section (Figure 3b), an instability during the steady-state simulation and a non-physical velocity distribution can be seen in the immediate vicinity of the fan. Neither the target quantity (velocity at selected reference points) nor the continuity residual (6e-2 to 1e-1) converged during the steady-state MRF calculation. The simulation model went through 20,000 iteration steps. Previous test simulations showed the same behavior even after 140,000 iteration steps.

Only with increasing distance to the fan, there is a better agreement with the expected flow characteristics from Wang, Zhang et al. (2019).

 DOI: 10.3217/978-3-85125-786-1-11 

*Table 2: Summary Error and Uncertainty [m/s]*

| | MEAN $u_D$ | MEAN ABSOLUTE ERROR (MAE) SIMULATION | | | | |
|---|---|---|---|---|---|---|
| | | V1 | V2 | V3 | V4 | V5 |
| whole section -0.8m...0.8m | 0.05 | 0.06 | 0.05 | 0.07 | 0.09 | 0.10 |
| center -0.1m...0.1m | 0.05 | 0.17 | 0.13 | 0.25 | 0.30 | 0.35 |
| outer zone 0.2m...0.5m -0.2m…-0.2m | 0.08 | 0.04 | 0.03 | 0.05 | 0.06 | 0.08 |

As shown in Peng et al. (2019) the MRF approach is sensitive to size and flow rate of the rotating zone, in order to include the tailing vortexes. In figure 3a, it can be seen, that the non-physical behavior of the MRF approach can be obviated, if the rotating zone is enlarged and fan rotation reduced. But this is only applicable, if no stationary parts exist in the near region of the fan like the housing or panel.

Consequently, it can be assumed that the transient phenomenon of the rotating ceiling fan cannot be adequately represented by means of steady-state calculation if obstacles, such as a panel opening or baffles, are present in the immediate vicinity of the fan. This complies also with results in Franzke et al. (2019).

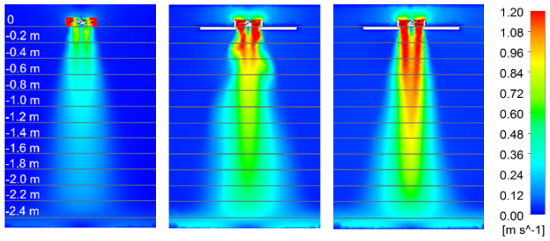


a b c

*Figure 3: Section mean velocity, a: freely suspended without housing and panel, with enlarged moving frame and reduced angular velocity (steady, coupled); b: V1, incl. housing and panel (steady, coupled); c: V4, incl. housing and panel (transient, coupled)*

Comparing results in figure 2, it can be seen that there are only slight differences in the velocity distribution between the coupled solution and the SIMPLE pressure correction method. In the steady-state calculation, the velocities of the SIMPLE pressure correction method are slightly higher than those of the coupled solution. In the transient calculation this is reversed.

**Discussion**

In comparison to the measured values, all the considered simulation models predict higher core jet velocities at 1.1 m above the floor. With a measurement uncertainty of 0.05 m/s, the minimum MAE is 0.25 m/s for transient solutions and 0.13 m/s for steady solutions.

Possible reasons could be the model simplification regarding the fan model. E.g. flow resistance and eddy shedding caused by the protection grill has not been taken into account in the simulation model.

Consequently, the applied geometry simplifications could have contributed to the differences between simulation and experiment. So, the overprediction cannot be solely assigned to the transient RBM simulation.

In future studies a model including the protection cover will be investigated. The coupling of the Transition SST model (in the region close to the fan) with the Realizable *k*-ε model (in the free shear flow region) will also be analyzed and additional measurements in different heights will be taken to allow a quantitative evaluation of the flow pattern.

## SUMMARY

The stationary simulations show the lowest MAE compared with measurements at 1.1 m above the floor. However, non-physical fluctuations occur in the immediate vicinity of the fan and at the panel opening using the MRF approach with obstacles close to the panel. Therefore, modelling a panel-integrated ceiling fan cannot be carried out with sufficient precision using stationary simulation models. The transient models follow the flow characteristics described in literature the most, but they predict too high velocities in the jet center compared to measurements at 1.1 m above the floor. In the jet center of the transient models, the MAE is five times higher than the measurement uncertainty and exceeds the measured values by at least 41%.

## ACKNOWLEDGEMENT

The analysis and data collection were conducted within the project ID: 03ET1563D funded by the German Federal Ministry of Economics and Technology (BMWi)

## REFERENCES

Adeeb, E., A. Maqsood, A. Musthaq, & Sohn, C. H. (2016). Parametric Study and Optimization of Ceiling Fan Blades for Improved Aerodynamic Performance. *Journal of Applied Fluid Mechanics*, *Vol 9*, 2905–2916.

ANSYS. (2017). *Fluent Theory Guide 18.2*.

Arens, E., Turner, S., Zhang, H [Hui], & Paliaga, G. (2009). Moving air for comfort. *ASHRAE Journal UC Berkeley: Center for the Built Environment*, 18–28.

ASHRAE. (2018). *Ashrae Standard 216P - Methods of Test for Determining Application Data of Overhead Circulator Fans*. ASHRAE.

ASHRAE Standard 55-2017. *ASHRAE Standard 55 - 2017 Thermal Environmental Conditions for Human Occupancy*. ASHRAE.

 DOI: 10.3217/978-3-85125-786-1-11 

ASME V&V. (2009). *Standard for verification and validation in computational fluid dynamics and heat transfer: An American national standard* (Reaffirmed 2016). *ASME V&V: 20-2009*. The American Society of Mechanical Engineers.

Aynsley, R. (2007). Circulating fans for summer and winter comfort and indoor energy efficiency. *Environment Design Guide*(25), 1–9.

Babich, F., Cook, M., Loveday, D., Rawal, R., & Shukla, Y. (2017). Transient three-dimensional CFD modelling of ceiling fans. *Building and Environment*, *123*, 37–49.

Bassiouny, R., & Korah, N. S. (2011). Studying the features of air flow induced by a room ceiling-fan. *Energy and Buildings*, *43*(8), 1913–1918.

Brager, G., Paliaga, G., & de Dear, R. (2004). *Operable windows, personal control and occupant comfort* (ASHRAE Transactions Vol 110 Teil 2 - 4695 (RP-1161)).

Candas, V., Libert, J. P., & Vogt, J. J. (1979). Influence of air velocity and heat acclimation on human skin wettedness and sweating efficiency. *Journal of Applied Physiology*(6), 1194–1200.

Casseer, D., & Ranasinghe, C. (2019). Assessment of Spallart Almaras Turbulence Model for Numerical Evaluation of Ceiling Fan Performance. *Moratuwa Engineering Research Conference*.

Chen, W., Liu, S [Shichao], Gao, Y., Zhang, H [Hui], Arens, E., Zhao, L., & Liu, J. (2018). Experimental and numerical investigations of indoor air movement distribution with an office ceiling fan. *Building and Environment*, *130*, 14–26.

de Dear, R., & Brager, G. (1998). *Developing an Adaptive Model of Thermal Comfort and Preference* (SF-98-7-3 (4106) (RP-884)).

DIN EN 16798-1:2015-Draft (2015). *Energy performance of buildings - Part 1: Indoor environmental input parameters for design and assessment of energy performance of buildings addressing indoor air quality, thermal environment, lighting and acoustics - Module M1-6; German and English version*. Beuth.

DIN EN ISO 7730:2006-05. *Ergonomics of the thermal environment - Analytical determination and interpretation of thermal comfort using calculation of the PMV and PPD indices and local thermal comfort criteria*.

EN ISO 7726:2001. *Ergonomics of the thermal environment - Instruments for measuring physical quantities; German version*.

Fanger, P. O. (1970). *Thermal Comfort: Analysis and applications in environmental engineering*. Danish Technical Press.

Franzke, R., & Sebben, S. (2018). *Validation of Different Fan Modelling Techniques in Computational Fluid Dynamics*. 21st Australasian Fluid Mechanics Conference, Adelaide.

Franzke, R., Sebben, S., Bark, T., Willeson, E., & Broniewicz, A. (2019). Evaluation of the Multiple Reference Frame Approach for the Modelling of an Axial Cooling Fan. *Energies*, *12*(15), 2934.

Gao, Y., Zhang, H [Hui], Arens, E., Present, E., Ning, B., Zhai, Y., Pantelic, J., Luo, M., Zhao, L., Raftery, P., & Liu, S [Shichao] (2017). Ceiling fan air speeds around desks and office partitions. *Building and Environment*, *124*, 412–440.

Glahn, O. (2016). *Instationäre Raumluftströmung zur Komfortoptimierung – Simulationsstudie zur Bewertung der durch Deckenventilatoren erzeugten Raumluftströmung* [Masterarbeit]. Technische Hochschule Ostwestfalen Lippe, Detmold.

Huang, L., Ouyang, Q., Zhu, Y., & Jiang, L. (2013). A study about the demand for air movement in warm environment. *Building and Environment*, *61*, 27–33.

DIN EN 15251:2012-12. *Indoor environmental input parameters for design and assessment of energy performance of buildings addressing indoor air quality, thermal environment, lighting and acoustics; German version*. Beuth.

Kim, J., Bauman, F., Raftery, P., Arens, E., Zhang, H [Hui], Fierro, G., Andersen, M., & Culler, D. (2019). Occupant comfort and behavior: High-resolution data from a 6-month field study of personal comfort systems with 37 real office workers. *Building and Environment*, *148*, 348–360.

Lin, H.-H. (2019). Improvement of Human Thermal Comfort by Optimizing the Airflow Induced by a Ceiling Fan. *Sustainability*, *11*(12), 3370.

Lin, S.-C., & Hsieh, M.-Y. (2014). An Integrated Numerical and Experimental Analysis for Enhancing the Performance of the Hidden Ceiling Fan. *Advances in Mechanical Engineering*. Advance online publication.

Liu, S [Shuo], Le Yin, Schiavon, S., Ho, W. K., & Ling, K. V. (2018). Coordinate control of air movement for optimal thermal comfort. *Science and Technology for the Built Environment*, *24*(8), 886–896.

Liu, S [Shuo], Lipczynska, A., Schiavon, S., & Arens, E. (2018). Detailed experimental investigation of air speed field induced by ceiling fans. *Building and Environment*, *142*, 342–360.

Luo, M., Cao, B., Ji, W., Ouyang, Q., Lin, B., & Zhu, Y. (2016). The underlying linkage between personal control and thermal comfort: Psychological or physical effects? *Energy and Buildings*, *111*, 56–63.

Melikov, A. K. (2004). Personalized ventilation. *Indoor Air*(14), 157–167.

Momoi, Y., Sagara, K., Yamanaka, T., & Kotani, H. (2004). *Modeling of Ceiling Fan Based on Velocity*

 DOI: 10.3217/978-3-85125-786-1-11 

*Measurement for CFD Simulation of Airflow in Large Room*.

Nicol, F., & Humphreys, M. A. (2002). Adaptive thermal comfort and sustainable thermal standards for buildings. *Energy and Buildings*, *34*(6), 563–572.

Oertel, H., & Prandtl, L. (2017). *Prandtl - Führer durch die Strömungslehre: Grundlagen und Phänomene* (14. Auflage). *Springer Reference Technik*.

Pasut, W., Arens, E., Zhang, H [Hui], & Zhai, Y. (2014). Enabling energy-efficient approaches to thermal comfort using room air motion. *Building and Environment*, *79*, 13–19.

Peng, W., Li, G., Geng, J., & Yan, W. (2019). A strategy for the partition of MRF zones in axial fan simulation. *International Journal of Ventilation*, *18*(1), 64–78.

Raftery, P., Fizer, J., Chen, W., He, Y., Zhang, H [Hui], Arens, E., Schiavon, S., & Paliaga, G. (2019). Ceiling fans: Predicting indoor air speeds based on full scale laboratory measurements. *Building and Environment*, *155*, 210–223.

Rissetto, R., Schweiker, M., & Wagner, A. (2020). The effects of occupants' expectations on thermal comfort under summer conditions. *11th Windsor Conference*.

Rizk, A., El-Deberky, A., & Guirguis, N. M. (2015). Simulation Comparison Between Natural and Hybrid Ventilation by Fans at Nighttime for Severe Hot Climate (Aswan, Egypt). In A. Sayigh (Ed.), *Renewable energy in the service of mankind: Selected topics from the World Renewable Energy Congress WREC 2014* (pp. 609–620). Springer.

Rohles, F. H., Konz, S. A., & Jones, B. W. (1982). *Ceiling Fans as Extenders of the Summer Comfort Envelope*. D-AC-2752.

Schiavon, S., & Melikov, A. K. (2008). *Energy saving and improved comfort by increasing air movement.* Center for Environmental Design Research.

Schiavon, S., & Melikov, A. K. (2009). Introduction of a Cooling-Fan Efficiency Index. *HVAC&R Research*, *15*(6), 1121–1144.

Schwarze, R. (2013). *CFD-Modellierung: Grundlagen und Anwendungen bei Strömungsprozessen*. Springer Vieweg.

Schweiker, M., & Wagner, A. (2016). The effect of occupancy on perceived control, neutral temperature, and behavioral patterns. *Energy and Buildings*, *117*, 246–259.

Shih, T.-H., Liou, W. W., Shabbir, A., Yang, Z., & Zhu, J. (1995). A new k-ϵ eddy viscosity model for high reynolds number turbulent flows. *Computers & Fluids*, *24*(3), 227–238.

Tanabe, S.-I., & Kimura, K.-i. (1994). Effects of Air Temperature, Humidity, and Air Movement on Thermal Comfort under Hot and Humid Conditions. In *ASHRAE Transactions* (pp. 953–969). ASHRAE.

Voss, K., & Voß, T. (2016). Integrated design approach for improving personal summer thermal comfort in existing office buildings with suspended ceilings.

Voss, K., Voß, T., Otto, J., Schweiker, M., & Rodriguez-Ubinas, E. (2013). *Investigation of ceiling fans for improving summer thermal comfort.* 2nd Central European Symposium on Building Physics. 2nd Central European Symposium on Building Physics, Wien, Österreich.

Wang, H., Luo, M., Wang, G., & Li, X. (2019). Airflow pattern induced by ceiling fan under different rotation speeds and blowing directions. *Indoor and Built Environment*, *158*, 1420326X1989005.

Wang, H., Zhang, H [Hong], Hu, X., Luo, M., Wang, G., Li, X., & Zhu, Y. (2019). Measurement of airflow pattern induced by ceiling fan with quad-view colour sequence particle streak velocimetry. *Building and Environment*, *152*, 122–134.

Xia, Y. Z., Niu, J. L., Zhao, R. Y., & Burnett, J. (2000). Effects of Turbulent Air on Human Thermal Sensations in a Warm Isothermal Environment. *Indoor Air*(10), 289–296.

Yakhot, V., Orszag, S. A., Thangam, S., Gatski, T. B., & Speziale, C. G. (1992). Development of turbulence models for shear flows by a double expansion technique. *Physics of Fluids a: Fluid Dynamics*, *4*(7), 1510–1520.

Zhai, Y., Arens, E., Elsworth, K., & Zhang, H [Hui] (2017). Selecting air speeds for cooling at sedentary and non-sedentary office activity levels. *Building and Environment*, *122*, 247–257.

Zhang, Y., & Zhao, R. (2007). Effect of local exposure on human responses. *Building and Environment*, *42*(7), 2737–2745.

Zhang, Z., Zhang, W., Zhai, Z. J., & Chen, Q. Y. (2007). Evaluation of Various Turbulence Models in Predicting Airflow and Turbulence in Enclosed Environments by CFD: Part 2—Comparison with Experimental Data from Literature. *HVAC&R Research*, *13*(6), 871–886.

Zhu, S., Srebric, J., Rudnick, S., N., Vincent, R., L., & Nardell, E., A. (2014). Numerical modeling of indoor environment with a ceiling fan and an upper-room ultraviolet germicidal irradiation system. *Building and Environment*(72), 116–124.

 DOI: 10.3217/978-3-85125-786-1-11 